Evolution of equatorial ionospheric plasma bubbles and formation of broad plasma depletions measured by the C/NOFS satellite during deep solar minimum

Chao-Song Huang,[1] O. de La Beaujardiere,[2] P. A. Roddy,[2] D. E. Hunton,[2] R. F. Pfaff,[3] C. E. Valladares,[1] and J. O. Ballenthin[2]

Received 30 July 2010; revised 23 November 2010; accepted 4 January 2011; published 8 March 2011.

[1] An unexpected feature revealed by the measurements of the Communication/Navigation Outage Forecasting System (C/NOFS) satellite is the presence of broad plasma depletions in the midnight–dawn sector during deep solar minimum. It has not been well understood what causes the broad plasma depletions and how equatorial plasma bubbles are related to the broad depletions. In this paper we present the C/NOFS measurements of equatorial plasma bubbles and broad depletions in a few cases. The ion density perturbations and enhanced ion vertical velocity are first identified in the topside *F* region at ~2200 LT, suggesting that the plasma bubbles start to form earlier at lower altitudes. The observations show that the plasma bubbles observed in the midnight–dawn sector may originate in the evening sector. The plasma bubbles continue growing for more than 3.3 h, and the decay time of the bubbles is also longer than 3.3 h. The continuous growth of the plasma bubbles in the evening sector and the slow decay after midnight determine that most plasma bubbles become fully developed and are easily detected in the midnight–dawn sector. The plasma flow inside the bubbles remains strongly upward throughout the entire nighttime. We propose the following mechanism for the generation of wide plasma bubbles and broad depletions. A series of plasma bubbles is generated through the Rayleigh-Taylor instability process over a large longitudinal range. These plasma bubbles grow and merge to form a wide bubble (width of ~700 km as observed), and multiple regular and/or wide bubbles can further merge to form broad plasma depletions (thousands of kilometers in longitude). The ion vertical drift inside each plasma bubble is driven by the polarization electric field and remains large after the bubbles have merged. This mechanism provides a reasonable interpretation of the large upward ion drift velocity inside the broad depletion region.

Citation: Huang, C.-S., O. de La Beaujardiere, P. A. Roddy, D. E. Hunton, R. F. Pfaff, C. E. Valladares, and J. O. Ballenthin (2011), Evolution of equatorial ionospheric plasma bubbles and formation of broad plasma depletions measured by the C/NOFS satellite during deep solar minimum, *J. Geophys. Res.*, *116*, A03309, doi:10.1029/2010JA015982.

1. Introduction

[2] The term "plasma bubble" is used to describe a region in the nighttime equatorial ionosphere within which the plasma density is significantly reduced. *Woodman and LaHoz* [1976] first reported Jicamarca coherent scatter radar observations of plume-like ionospheric structures. They suggested that the plumes represent depleted plasma density regions (plasma bubbles). Equatorial plasma bubbles have been extensively studied since then in radar measurements [*Tsunoda and White*, 1981; *Tsunoda*, 1983; *Kudeki and Bhattacharyya*, 1999; *Fejer et al.*, 1999], in satellite experiments [*Hanson and Bamgboye*, 1984; *Aggson et al.*, 1992; *Burke et al.*, 2003], in rocket experiments [*Kelley et al.*, 1982, 1986; *LaBelle and Kelley*, 1986], and by other measurements [*Abdu et al.*, 2003; *Sahai et al.*, 2005]. Plasma bubbles can ascend to thousands of kilometers at their apex, and the depleted density regions can extend into middle latitudes along the geomagnetic field lines [*Burke et al.*, 1979; *Kelley et al.*, 2003; *Makela and Kelley*, 2003; *Huang et al.*, 2007; *de La Beaujardiere et al.*, 2009].

[3] The physical mechanism for the generation of plasma bubbles in the equatorial ionosphere has been well understood. Plasma bubbles are generated through the nonlinear evolution of the Rayleigh-Taylor instability [*Haerendel*, 1973]. The Rayleigh-Taylor instability is excited in the bottomside *F* region and evolves into a plasma bubble that penetrates the *F* peak to the topside *F* region. Numerical

[1]Institute for Scientific Research, Boston College, Chestnut Hill, Massachusetts, USA.
[2]Air Force Research Laboratory, Hanscom Air Force Base, Massachusetts, USA.
[3]NASA Goddard Space Flight Center, Greenbelt, Maryland, USA.

Copyright 2011 by the American Geophysical Union.
0148-0227/11/2010JA015982

simulations have reproduced the generation and evolution of plasma bubbles [*Scannapieco and Ossakow*, 1976; *Zalesak et al.*, 1982; *Huang and Kelley*, 1996a, 1996b; *Keskinen et al.*, 2003; *Keskinen and Vadas*, 2009; *Huba and Joyce*, 2007; *Huba et al.*, 2009a, 2009b; *Krall et al.*, 2010a, 2010b; *Retterer*, 2010a, 2010b]. The plasma density inside the bubbles can be decreased by 1 to 3 orders of magnitude.

[4] Whether seed perturbations exist in the bottomside *F* region is an important factor that influences the generation of plasma bubbles. *Rottger* [1973] reported observations of large-scale structures of *F* region irregularities and suggested that the wavelike structures were produced by atmospheric gravity waves. *Kelley et al.* [1981] suggested that growth from thermal noise is unlikely to lead to the large-scale equatorial plasma bubbles because of the low growth rate of the Rayleigh-Taylor instability and that the quasiperiodic ionospheric plumes observed by radars may be seeded by gravity waves with the same periodicity. *Huang et al.* [1993] analyzed the gravity wave initiation of the plasma instability via spatial resonance and showed that the instability grows and amplifies the gravity wave-induced perturbations, resulting in the formation of plasma bubbles. The numerical simulations of *Huang and Kelley* [1996a, 1996b] reproduced these processes. Recent observations show that plasma bubbles can be indeed related to gravity waves [*Abdu et al.*, 2009; *Takahashi et al.*, 2009; *Makela et al.*, 2010]. Besides gravity waves, *Hysell et al.* [2005a, 2005b, 2006] and *Kudeki et al.* [2007] suggested that vertical shear in the zonal plasma drift in the bottomside *F* region causes wave-like structures. These structures appear to be able to seed ionospheric interchange instabilities and initiate equatorial spread *F*.

[5] Note that a plasma bubble is also termed plasma depletion when the decrease of the plasma density is addressed. Because the typical width of a fully developed plasma bubble is ~100 km in longitude, we use the term "plasma bubble" to describe the plasma density decrease over a relatively small range (e.g., tens to hundreds of kilometers in longitude). The term, 'wide bubbles', is used specifically for the plasma density decreases over several hundreds of kilometers in longitude. If the plasma density decreases occur over a very large longitudinal range (e.g., greater than 1000 km), they are not the conventional bubbles and are termed "broad plasma depletions" in this paper.

[6] The Communication/Navigation Outage Forecasting System (C/NOFS) satellite [*de La Beaujardiere et al.*, 2004] was launched in April 2008. Its scientific objectives are to understand the physical processes that lead to the formation of plasma bubbles and plumes in the nighttime equatorial ionosphere. C/NOFS has been providing continuous measurements of the low-latitude ionospheric ion density, ion drift velocity, and electric fields. An unexpected feature revealed by the C/NOFS measurements is the presence of broad plasma depletions near dawn [*Burke et al.*, 2009; *de La Beaujardiere et al.*, 2009; *Huang et al.*, 2009; *Kelley et al.*, 2009; *Su et al.*, 2009].

[7] Different mechanisms have been proposed to explain the generation of the broad plasma depletions. *Huang et al.* [2009] suggested that the formation of the broad plasma decreases could be related to a cooling or downwelling of the ionosphere and thermosphere in the equatorial region; they ruled out the possibility of plasma bubbles as the cause. *Huba et al.* [2010], using numerical simulations of the ionospheric model SAMI3, found that a postmidnight enhancement of the eastward electric field can cause the formation of the equatorial plasma depletions near dawn. The effect of the eastward electric field is similar to equatorial fountain and is also not involved with plasma bubbles. The broad plasma depletions are independent from equatorial plasma bubbles in both mechanisms.

[8] On the other hand, C/NOFS often detects equatorial plasma bubbles besides broad depletions, and the upward ion drift velocity is 100–300 m s^{-1} inside the bubbles. It has not been understood how individual plasma bubbles are related to the broad plasma depletions, where the plasma bubbles and depletions start to occur, and why most plasma bubbles and depletions are observed near dawn. In this study, we analyze the generation and evolution of plasma bubbles and propose a new causal mechanism of the broad plasma depletions near dawn.

2. Observations

[9] C/NOFS is a low-inclination (13°) satellite, with orbital period of 100 min. The orbit of C/NOFS can be very close to the magnetic equator over a large longitudinal range. If an equatorial plasma bubble exists for longer than 100 min, the bubble can be detected by successive passages of C/NOFS. Therefore, C/NOFS is able to measure the growth and evolution of long-lasting plasma bubbles.

[10] We present the ion density and ion vertical velocity measured by the C/NOFS satellite over six successive orbits on 18 August 2008 in Figure 1. Figure 1a shows the latitude and altitude of C/NOFS, Figure 1b shows the ion density, and Figure 1c shows the ion vertical velocity. The ion density and ion velocity during each orbit are plotted in the same row. For each orbit, the orbit number is given in Figure 1a, and the UT interval during which C/NOFS flies over the local time range of 2000–0600 is given in Figure 1b. All data are plotted as a function of solar local time at the satellite position. The shift of continents from one orbit to next corresponds to the rotation of the Earth. The ion vertical velocity in Figure 1c is calculated from the electric field measured by the Vector Electric Field Instrument (VEFI) on board C/NOFS [*Pfaff et al.*, 2010]. We have converted the electric field into ion drift velocity to show the plasma movement. For the VEFI data, the "vertical" direction (termed as "meridional" in the VEFI data system) is defined as the vector product of the zonal direction and the direction of the magnetic field. This direction is vertical at the magnetic equator and may become slightly different from, but still close to, the vertical direction at off-equatorial positions.

[11] We first analyze the plasma bubble marked by the yellow bar. During orbit 1830 (the top row of Figure 1), C/NOFS detects an ion density enhancement at ~2030 LT. C/NOFS is located at 8° magnetic latitude (MLat), and its altitude is 620 km (see Figure 1a). Plasma enhancements associated with equatorial plasma bubbles can be generated at off-equatorial locations [*Le et al.*, 2003; *Krall et al.*, 2010b] and just above the upper boundary of the plasma depletion [*Retterer*, 2010a]. In both processes, the ion vertical velocity inside the density enhancement region is increased. However, the ion vertical velocity in the density

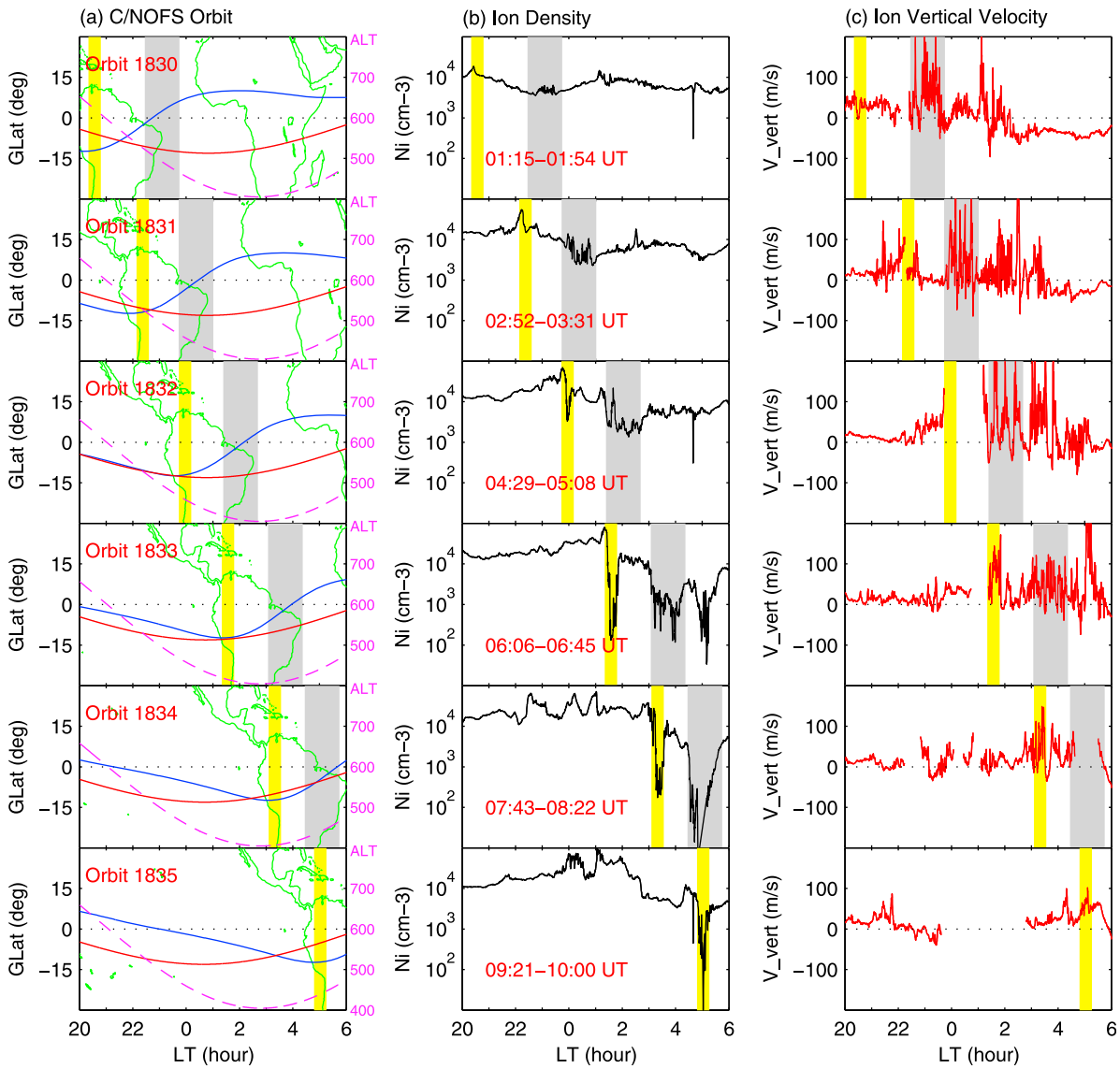

Figure 1. (a) Low-latitude ionospheric ion density and ion vertical velocity measured by the C/NOFS satellite on 18 August 2008. The green line depicts the continents, the blue line depicts the magnetic equator, the red line represents the latitude of C/NOFS, and the dashed magenta line represents the altitude (in kilometers) of C/NOFS labeled on the right. (b) The ion density and (c) ion vertical velocity are plotted. The yellow shading denotes a plasma bubble, and the gray shading denotes a broad plasma depletion.

enhancement region is nearly the same as that in the background plasma during orbit 1830. It cannot be determined whether the plasma enhancement at ~2030 LT is related to an equatorial plasma bubble.

[12] During orbit 1831, the density enhancement near the west coast of South America is again detected when C/NOFS is very close to the magnetic equator, and the ion density starts to decrease at the eastern edge of the enhancement. The ion vertical velocity in the density enhancement region becomes ~100 m s^{-1}, much higher than the background plasma drift. The large upward ion velocity at ~2210 LT is consistent with the Rayleigh-Taylor instability process [*Le et al.*, 2003; *Krall et al.*, 2010b; *Retterer*, 2010a] and can be considered as the signature of the instability. In other words, the plasma bubble, or its signature, caused by the Rayleigh-Taylor instability has reached the altitude of C/NOFS during orbit 1831. The C/NOFS measurements are made at 527 km altitude, above the *F* peak. The Rayleigh-Taylor instability should have been excited in the bottomside *F* region at an earlier time, before 2210 LT.

[13] A plasma bubble becomes very clear at ~0000 LT during orbit 1832. This bubble appears to grow from the density decrease at the eastern edge of the ion density enhancement during orbit 1831. The plasma bubble becomes well developed at ~0140 LT during orbit 1833. The ion density inside the bubble is decreased by more than 2 orders of magnitude, and the ion vertical velocity is 100–150 m s^{-1}. The plasma bubble at that longitude is also detected by C/NOFS through orbits 1834 and 1835.

[14] The ambient ion density shows a broad minimum at ~0500 LT during orbit 1831. No plasma bubble activity occurs there, and the ion vertical velocity is downward and

does not change much between 0400 and 0600 LT. This density minimum represents the normal variation with local time. In contrast, the ion density inside the bubble at ~0500 LT during orbit 1835 is decreased by 2–3 orders of magnitude, and the ion vertical velocity is ~100 m s^{-1} and upward. The large plasma reductions with enhanced upward plasma flow near dawn are plasma bubbles.

[15] In order to understand why the plasma bubble starts to occur in the evening sector, we examine the vertical velocity during orbits 1830 and 1831. Note that the ion velocity (electric field) is measured at different latitudes and altitudes. The latitudinal range of the C/NOFS orbit is ±13° geographic. Because of the offset between geographic and geomagnetic latitudes, the C/NOFS orbit varies between ±23° in magnetic latitude. The altitude range of the C/NOFS orbit is 405–845 km. The ion velocity in this study has not been normalized to the magnetic equator or to a single altitude. The analysis of the VEFI data by *Pfaff et al.* [2010] shows that the average pattern of the electric field measured by the VEFI is consistent with the pattern derived from the Jicamarca radar measurements. The variation of the ion vertical drift with local time along the satellite track should approximately represent the variation over the magnetic equator. The ion vertical velocity is 40–50 m s^{-1} at ~1800 LT and remains upward in the evening sector (1800–2100 LT); the data before 2000 LT are not plotted in Figure 1. The upward plasma drift moves the *F* region to high altitudes conducive to the generation of the plasma bubble.

[16] We want to emphasize that the orbit of C/NOFS is very suitable for tracing the evolution of the plasma bubble. C/NOFS is at, or very close to, the magnetic equator when it flies over the west coast of South America during four successive orbits (1831–1834) in this case, and its altitude varies in the range of 400–600 km. In particular, C/NOFS does not detect other major depletions, except for the one marked by the yellow shading, over the Pacific Ocean and South America. The existence of an isolated plasma bubble over a large longitudinal range excludes the possibility that each C/NOFS orbit detects a different bubble. The shift of the bubble in local time is caused primarily by the Earth's rotation. The region of the bubble has rotated to the morning sector (after 0600 LT) during orbit 1836. The zonal drift of plasma bubbles causes the change of the position (longitude) of the bubbles and will be discussed later.

[17] We estimate the duration during which the plasma bubble is growing. The linear growth time of the Rayleigh-Taylor instability is the reciprocal of the linear growth rate and must be short (e.g., ~15 min) for the instability to grow into a plasma bubble. However, a plasma bubble is not expected to form within the linear growth time. The Rayleigh-Taylor instability undergoes first linear growth and then nonlinear growth to form a topside plasma bubble. Simulations show that the plasma perturbations caused by the Rayleigh-Taylor instability take, in general, 30–60 min to penetrate the *F* peak, depending on the altitude profile of the *F* region plasma and other parameters [*Scannapieco and Ossakow*, 1976; *Zalesak et al.*, 1982; *Huang and Kelley*, 1996a, 1996b; *Keskinen et al.*, 2003; *Keskinen and Vadas*, 2009; *Huba and Joyce*, 2007; *Huba et al.*, 2009a, 2009b; *Krall et al.*, 2010a, 2010b; *Retterer*, 2010a, 2010b]. Furthermore, a plasma bubble, after penetrating the *F* peak, continues to move upward and to grow to a larger size in the zonal/longitudinal direction. The simulations of *Huba et al.* [2009a] and *Krall et al.* [2010a] show that a plasma bubble continuously grows and ascends for ~4 h. Note that the growth time discussed here is not the linear growth time of the Rayleigh-Taylor instability. The growth time of a plasma bubble includes the linear and nonlinear growth of the Rayleigh-Taylor instability and the resultant bubble. Because the orbit of C/NOFS is in the topside *F* region, we cannot determine the time when the instability is excited in the bottomside *F* region and the time when the bubble reaches the maximum altitude from the C/NOFS data alone.

[18] Instead, we examine the size of a plasma bubble in the longitudinal direction. The bubble is still growing if it becomes wider and deeper. The signature of the plasma bubble/Rayleigh-Taylor instability in the case of Figure 1 is detected by C/NOFS at ~2210 LT during orbit 1831, and a well developed, wide bubble is detected at ~0140 LT during orbit 1833. As will be discussed later, the wide bubble may result from merging of several bubbles with smaller size. The smaller bubbles, or the single wide bubble, must be growing for the merging to occur. The observations suggest that the plasma bubble grows over two complete orbits (3.3 h). Because the Rayleigh-Taylor instability must have been excited at earlier time than it reaches the C/NOFS altitude, the growth time of the plasma bubble is longer than 3.3 h.

[19] Similarly, we can estimate how long the plasma bubble takes to decay. The plasma bubble becomes the deepest and widest during orbit 1833, and its size does not grow after that time. The plasma particles inside the bubble are still moving upward during orbits 1834–1835. The plasma bubble does not significantly decay and does not become a dead/fossil bubble over two complete orbits (3.3 h). When the bubble approaches dawn, the newly produced electrons and ions by photoionization rapidly fill the depleted region, so the bubble disappears there. The decay time of the plasma bubble is also longer than 3.3 h.

[20] We now discuss the broad plasma depletion denoted by the gray bar in Figure 1. C/NOFS detects ion density enhancements and large upward ion vertical velocity (100–200 m s^{-1}) between −10° and −23° MLat during orbit 1830, as shown in the top row of Figure 1. The large upward ion velocity and ion density enhancements at the off-equator locations are consistent with the existence of equatorial plasma bubbles [*Le et al.*, 2003; *Krall et al.*, 2010b; *Retterer*, 2010a]. During orbit 1831, C/NOFS is closer to the magnetic equator and detects both increase and decrease of the ion density. The location of C/NOFS at this time should be near the boundary between the plasma density decrease in the equatorward side and the density enhancement in the poleward side. After that, C/NOFS detects decreases of the ion density in this longitude region during orbits 1832–1834. The ion density is reduced by 2–3 orders of magnitude over a longitudinal range of ~20° (2200 km) when this region reaches ~0500 LT. This is a typical example of broad plasma depletions observed by C/NOFS near dawn.

[21] An important feature of the plasma bubble denoted by the yellow bar in Figure 1 is the large size in the longitudinal direction. A plasma bubble is a region of depleted plasma. This depleted region is generally enclosed on three sides (top, east, and west) in the plane transverse to the magnetic field and extends along the magnetic field lines.

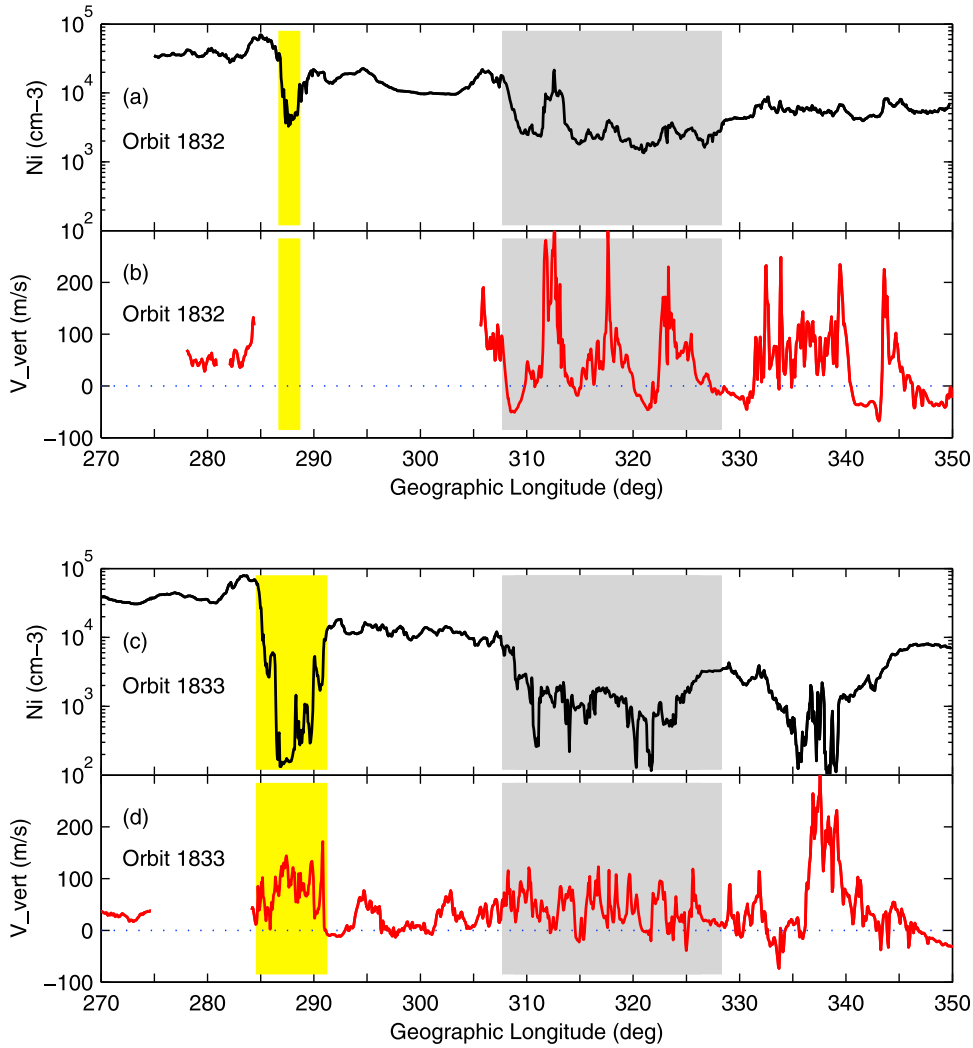

Figure 2. Longitudinal variations of the ion density and velocity during C/NOFS orbits 1832 and 1833 on 18 August 2008. The yellow shading denotes a plasma bubble, and the gray shading denotes a broad plasma depletion.

The three-dimensional structure of plasma bubbles has been well reproduced in numerical simulations [*Huba et al.*, 2009a; *Keskinen and Vadas*, 2009; *Krall et al.*, 2010a; *Retterer*, 2010a]. However, a satellite can make measurements only along its track. Because the orbit of C/NOFS is very close to the magnetic equator in this case, C/NOFS measures the variations of the plasma density in the west-east direction. The distance between the trailing and leading edge of the depleted region along the C/NOFS track represents the distance between the west and east wall of the plasma bubble. In other words, the distance is the width of the bubble in the zonal direction, rather than the extension of the bubble along the magnetic field lines.

[22] In order to show the detailed variations of the ionospheric parameters inside the plasma bubble and depletion, we replot the ion density and velocity during orbits 1832 and 1833 in Figure 2. We use the sharp decrease of the ion density from its background value to determine the boundary of the plasma bubble. The plasma bubble, denoted by the yellow shading, has a zonal/longitudinal width of ~1.6° (177 km) during orbit 1832 (Figure 2a). This plasma bubble becomes much wider and deeper during orbit 1833 (Figure 2c), and its width is ~6° (677 km). There is no ion velocity data in the bubble region during orbit 1832 (Figure 2b). The ion vertical velocity is ~100 m s^{-1} inside the wide bubble during orbit 1833 (Figure 2d).

[23] The broad plasma depletion is denoted by the gray shading in Figure 2. The longitudinal coverage of the plasma depletion is ~20° (2200 km). The ion vertical velocity inside the depletion region reaches 300 m s^{-1} during orbit 1832 and becomes ~100 m s^{-1} during orbit 1833. In particular, the ion vertical velocity inside the depletion region shows three peaks in Figure 2b, and each of the velocity enhancements covers 6–7° in longitude.

[24] As can be seen in Figure 1, the position (longitude) of the plasma bubble, denoted by the yellow shadings, is relatively constant. However, this does not mean that the plasma bubble is fixed in longitude. In fact, plasma bubbles and spread *F* irregularities move in the zonal direction [*Abdu et al.*, 1985; *Valladares et al.*, 1996; *Immel et al.*, 2003; *Park et al.*, 2007; *Huang et al.*, 2010]. The zonal drift of plasma bubbles is eastward (~100 m s^{-1}) at 1900–2000 LT,

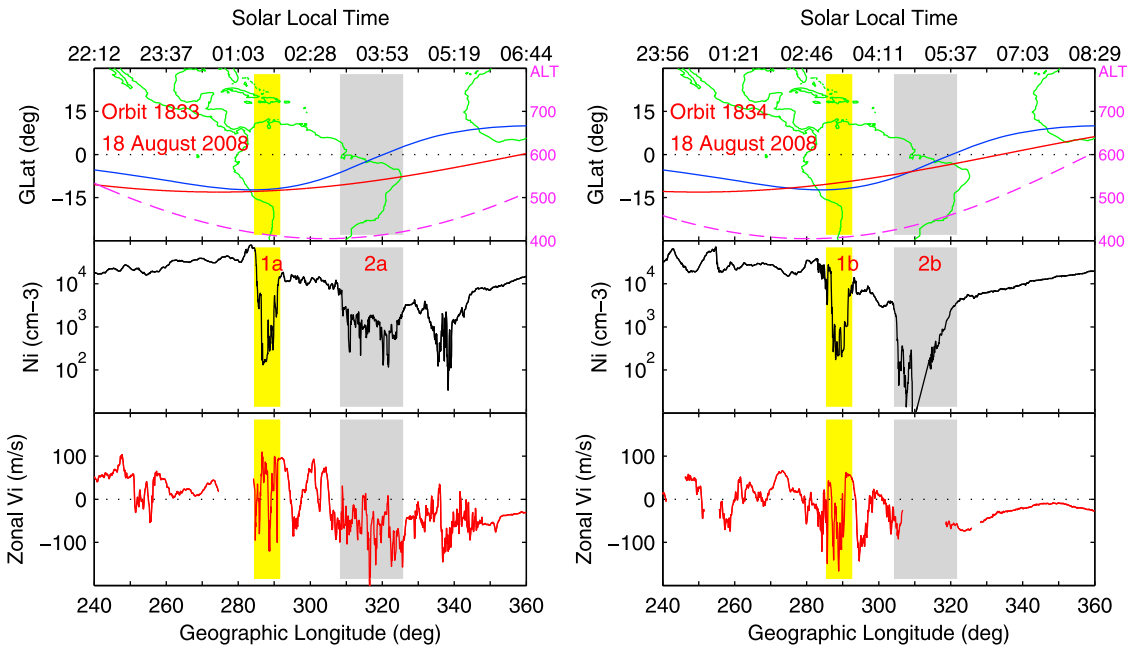

Figure 3. The ionospheric ion density and ion zonal velocity measured by C/NOFS during two successive orbits on 18 August 2008. The yellow and gray shadings denote the wide plasma bubble and the broad depletion, respectively. The zonal velocity is positive in the eastward direction. The solar local time is given at the top.

gradually decreases toward midnight, reverses direction at 0300–0400 LT, and becomes westward near dawn. The zonal drift of plasma bubbles is closely related to the ambient plasma drift but is generally higher than the background plasma drift [*Valladares et al.*, 1996; *Immel et al.*, 2003].

[25] In our case, a change of the position (longitude) of the plasma bubble indeed occurs and is caused by the zonal drift of the bubble. We use the C/NOFS measurements to estimate the zonal drift velocity of the plasma bubble. We plot in Figure 3 the ion density and ion zonal velocity during orbit 1833–1834. The plasma bubble and broad depletion are marked as 1a and 2a during orbit 1833 and as 1b and 2b during orbit 1834, respectively. We take the positions of the midpoint of the bubble to calculate the zonal drift velocity. If we assume that bubbles 1a and 1b are the same bubble, the zonal drift velocity is 18 m s^{-1} eastward. Similarly, we assume that depletions 2a and 2b are the same one and find that this depletion has a westward drift velocity of 40 m s^{-1}. Previous studies show that the zonal drift velocity of ESF irregularities and plasma bubbles is generally eastward and reverses to westward near dawn [*Abdu et al.*, 1985; *Valladares et al.*, 1996; *Immel et al.*, 2003; *Park et al.*, 2007; *Huang et al.*, 2010]. In our case, during the two orbits, the plasma bubble (1a, 1b) is located at 0100–0330 LT, and the broad depletion (2a, 2b) is located at 0330–0500 LT. A small eastward drift velocity for the bubble and a relatively large westward drift velocity for the depletion are consistent with the previous results. The bottom panels of Figure 3 show the ion zonal drift velocity measured by the VEFI on board C/NOFS. The zonal velocity of the background ions is generally eastward outside the bubble (yellow shading) and westward outside the depletion (gray shading). The direction and value of the zonal drift estimated from the change of the longitude of the bubble/depletion are consistent with the measured ambient plasma drift.

[26] The zonal drift velocity of plasma bubbles can be used to identify whether we are tracing the right bubble. If we use bubble 1a and bubble 2b to calculate the zonal drift velocity, the zonal velocity would be ~400 m s^{-1} eastward. Such a large eastward drift velocity is unrealistic for plasma bubbles in the midnight–dawn sector, so bubbles 1a and 2b are not the same bubble.

[27] We present another case in which the generation and evolution of plasma bubbles show similar characteristics. This case occurred on 7–8 June 2008, and the C/NOFS data are plotted in Figure 4. In this case, the plasma bubble is located near the east coast of the African continent, as denoted by the yellow bars. The position of this bubble is not fixed in longitude. The shape of the bubble does not change much between orbits 775 and 776, and the zonal drift velocity of the bubble is ~20 m s^{-1} eastward. This zonal drift velocity is reasonable.

[28] During orbit 772, the ion density and velocity do not show any obvious perturbations at the east coast of Africa. An increase of the ion density and a corresponding increase of the upward ion velocity are detected at ~2200 LT during orbit 773; C/NOFS is located at −6° MLat and at 446 km altitude. The enhanced ion density and ion velocity are likely to be the signature of a plasma enhancement caused by an equatorial plasma bubble [*Le et al.*, 2003; *Krall et al.*, 2010b; *Retterer*, 2010a]. During orbit 774, a narrow plasma bubble is detected by C/NOFS over the magnetic equator, and the ion upward velocity is ~200 m s^{-1} inside the bubble. The plasma bubble becomes fully developed at ~0110 LT during orbit 775, and the ion vertical velocity reaches 300 m s^{-1}. The plasma bubble is growing for 3.3 h between orbit 773 and 775. In addition, the Rayleigh-Taylor insta-

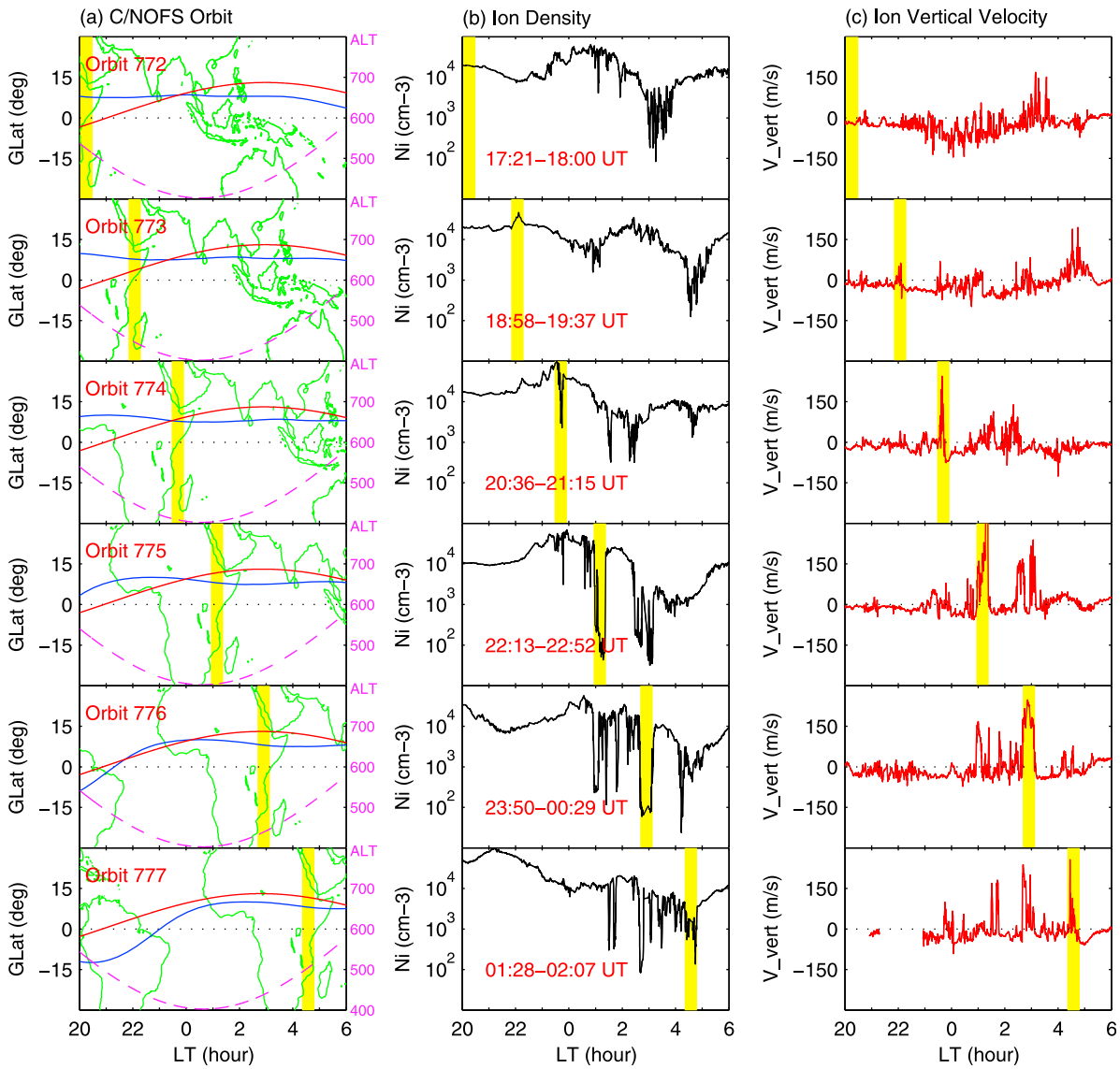

Figure 4. Same as Figure 1 but for the period from 1721 UT on 7 June 2008 to 0207 UT on 8 June 2008.

bility must have been excited before the signature of the bubble is detected by C/NOFS during orbit 773. Therefore, the growth time of the bubble is longer than 3.3 h. The ion vertical velocity remains strongly upward (~200 m s^{-1}) during orbits 776 and 777, and the bubble does not become a dead bubble when it reaches ~0430 LT. The decay time of the bubble is also longer than 3.3 h.

[29] The ion vertical velocity during orbits 772–777 is plotted in Figure 5a. The upward ion velocity is significantly enhanced between 1600 and 1900 LT during orbits 772 and 773. This increased upward drift near dusk may play a role similar to the prereversal enhancement [*Fejer et al.*, 1991, 2008] and cause the generation of the plasma bubble. The detailed variations of the ion density and velocity are plotted in Figures 5b and 5c for the local time range of 1800–2400. The yellow bar denotes the enhancements of the ion density and velocity during orbit 773. The gray bar denotes the same longitudinal region in the previous orbit (orbit 772). There is no obvious perturbation in the ion density and velocity during orbit 772. However, because C/NOFS is located at 523 km altitude at −12° MLat, it cannot detect plasma perturbations in the bottomside equatorial *F* region. It is uncertain whether there are initial perturbations in the bottomside *F* region for the excitation of the Rayleigh-Taylor instability.

[30] Figures 5d and 5e show the longitudinal variations of the plasma bubble during orbit 776. The ion density near the center of the bubble becomes smaller than the instrumental lower limit (100 cm^{-3}) and may not be reliable; we use a dotted line to denote this portion and do not show the data (Figure 5d). The ion vertical velocity, plotted in Figure 5e, has continuous data coverage and shows three peaks inside the bubble. The width of this plasma bubble is 6.3° (~700 km) in longitude.

[31] The plasma bubbles in the two cases of 18 August 2008 and 7–8 June 2008 start to grow in the evening sector and corotate with Earth to the postmidnight sector. This does not mean that all plasma bubbles observed in the

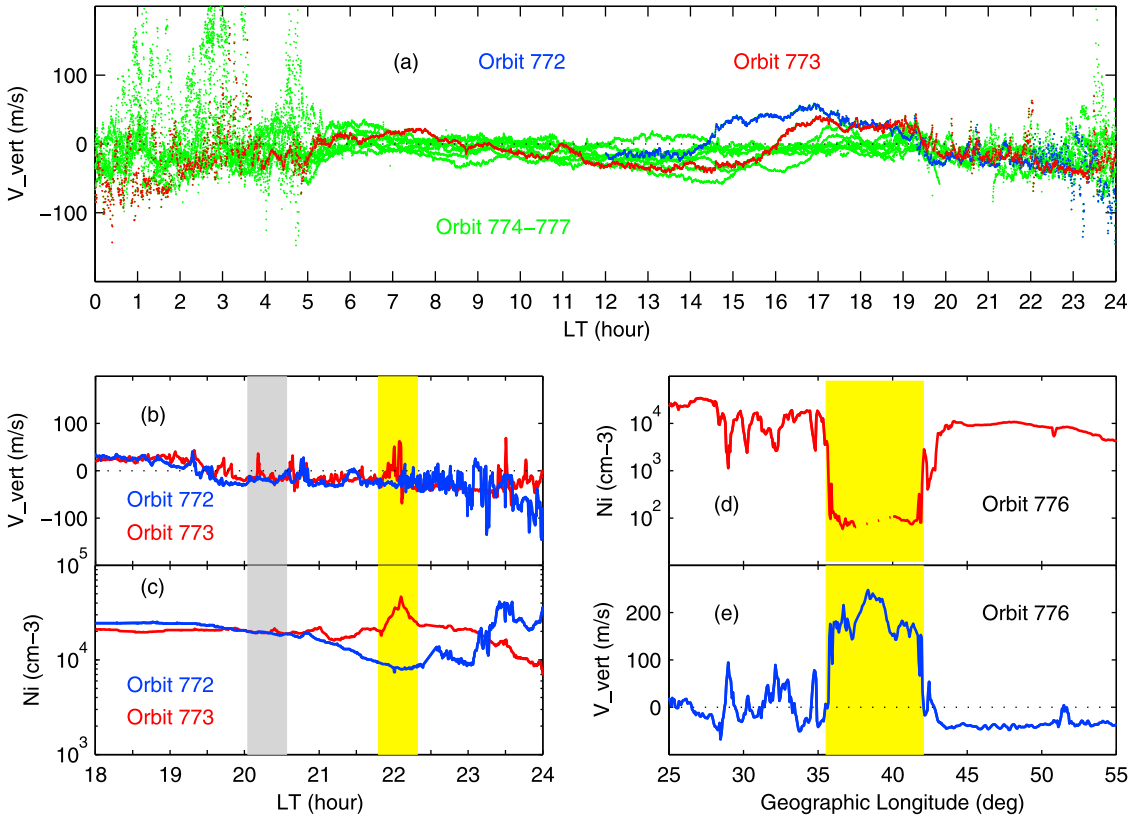

Figure 5. (a) Low-latitude ionospheric ion vertical velocity as a function of local time measured by the C/NOFS satellite during the period from 1721 UT on 7 June 2008 to 0207 UT on 8 June 2008. (b and c) The ion vertical velocity and ion density measured by C/NOFS in the local time range of 1800–2400. (d and e) The ion density measured by C/NOFS during orbit 776. The ion density is plotted as a function of longitude to show the longitudinal variations of the ion density and velocity.

postmidnight sector originate in the evening sector. Here we show an example in which the plasma bubble forms rapidly in the postmidnight sector. This case occurred on 13 June 2008, and the C/NOFS data are plotted in Figure 6. During orbit 851, C/NOFS detects only very small perturbations in the ion density and ion velocity near the west coast of the African continent, suggesting that no significant bubble structures exist at the moment. In contrast, a large plasma bubble is detected during orbit 852, and the ion vertical velocity inside the bubble reaches 300 m s^{-1}. The C/NOFS measurements during orbit 851 and 852 imply that this plasma bubble grows rapidly within the period of one complete orbit (~100 min). The plasma bubble corotates with Earth to ~0350 LT during orbit 853, and the ion vertical velocity is still larger than 300 m s^{-1}. If we take a closer look at the C/NOFS orbits in Figure 6a, we can see that the plasma bubble has moved westward between orbit 852 and 853. In other words, the plasma bubble has a westward drift velocity near dawn, consistent with the measurements in other cases. During orbit 854, the west coast of the African continent is at ~0600 LT, and a broader plasma depletion is located at ~0445 LT, as denoted by the gray bar. If the depletion at ~0445 LT during orbit 854 was the same bubble at ~0350 LT during orbit 853, the plasma bubble would have a westward drift velocity of 370 m s^{-1}. Such a large westward drift velocity is unrealistic, so the plasma depletion during orbit 854 is unlikely to be the plasma bubble during the previous orbit.

3. Discussion

[32] The C/NOFS satellite often detects plasma bubbles and broad plasma depletions in the midnight–dawn sector during the current deep solar minimum [*Burke et al.*, 2009; *de La Beaujardiere et al.*, 2009; *Huang et al.*, 2009; *Kelley et al.*, 2009]. *Miller et al.* [2010] analyzed the occurrence of equatorial plasma depletions observed by optical airglow images and coherent backscatter in the central Pacific sector. They found an increase in postmidnight equatorial irregularity/bubble activity during the recent solar minimum. Their findings are consistent with the broad plasma depletions detected by C/NOFS near dawn. This paper addresses where the postmidnight plasma depletions originate and how the depletions are formed. We have analyzed three cases. An enhanced upward plasma drift, similar to the prereversal enhancement, is an important factor that controls the generation of plasma bubbles in the evening sector. In the cases of 18 August 2008 and 7–8 June 2008, the ion vertical velocity is upward near 1800–1900 LT. The perturbations in the ion density and ion vertical velocity are first observed around 2200 LT. The observations show that the plasma bubbles start to form in the evening sector and become fully developed in the postmidnight sector. The

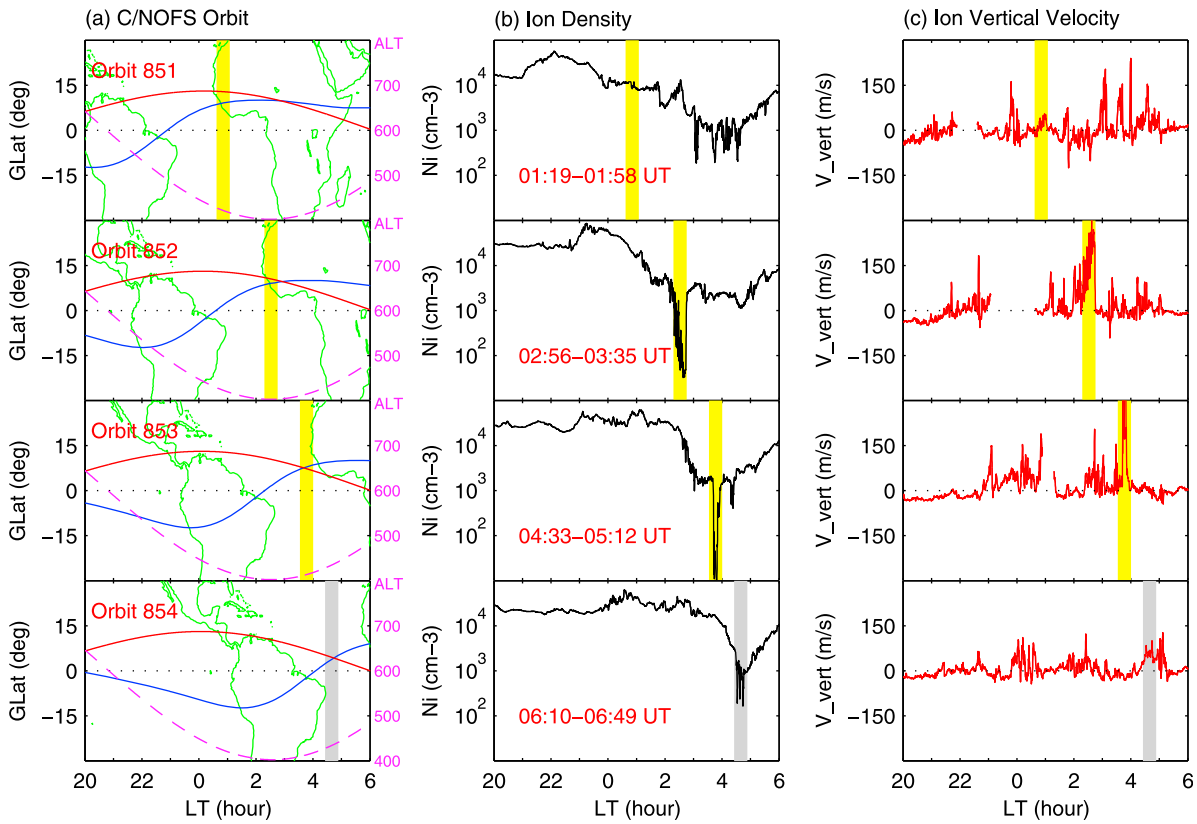

Figure 6. Same as Figure 1 but for 13 June 2008.

plasma bubble in the case of 13 June 2008 is generated in the postmidnight sector. In these cases, the south-north component of the interplanetary magnetic field (IMF) was fluctuating between −5 and 5 nT, the Dst index was larger than −30 nT, and no magnetic storm activity was involved. The plasma bubbles occurred during magnetic quiet times.

[33] The persistence of a plasma bubble is determined by the growth and decay time. The simulations of *Huba et al.* [2009a] and *Krall et al.* [2010a] show that the entire growth time of a plasma bubble, from the excitation of the Rayleigh-Taylor instability in the bottomside *F* region to the arrival of the bubble at the maximum altitude, is ~4 h. In both cases of Figures 1 and 4, the growth time of the plasma bubbles is longer than 3.3 h. The observed growth time is consistent with the simulations of *Huba et al.* [2009a] and *Krall et al.* [2010a].

[34] The width of a plasma bubble is the scale size of the bubble in the zonal direction, or the distance between the west and east wall/boundary of the bubble. A radar scan in the east-west direction is able to detect the spatial structure of plasma bubbles. The ALTAIR radar scans provide direct measurements of the width of plasma bubbles [*Tsunoda and White*, 1981; *Tsunoda et al.*, 1982; *Tsunoda*, 1983]; the typical width of a plasma bubble in the ALTAIR scan is tens of kilometers. Plasma bubbles with this size are reproduced by numerical simulations. For example, the width of the plasma bubble in the simulations of *Huba et al.* [2009a] is ~50 km below 1000 km and becomes ~150 km in the altitude range of 1000–2000 km. The simulations of *Retterer* [2010a] also show that the width of plasma bubbles is several tens of kilometers.

[35] C/NOFS can fly almost along the magnetic equator and measure the width of equatorial plasma bubbles. C/NOFS measurements show the existence of plasma bubbles over a large range of scale length in the zonal direction, including those with a characteristic width of tens of kilometers, similar to the radar measurements and simulations. A new finding of the C/NOFS measurements is the occurrence of unusually wide plasma bubbles. As shown in Figures 2 and 5, the width of the plasma bubbles can be as large as 667–700 km at the altitude of 400–500 km.

[36] We suggest the following mechanism for the generation of the wide plasma bubbles and broad plasma depletions. A series of equatorial plasma bubbles start to form in the bottomside *F* region over a broad longitude range (e.g., 10–30°) in the evening sector. Each of the bubbles is caused by the Rayleigh-Taylor instability process, and the polarization electric field inside the bubbles drives upward ion drift. During the growing and rising process, the bubbles become deeper, and the longitudinal size (width) of the bubbles becomes larger. When the width of individual bubbles becomes larger than the separation of the successive bubbles, two or more bubbles merge to form a wider bubble or broad plasma depletions. The merging process among the bubbles continues as they corotate with Earth toward the postmidnight sector. As a result, broad plasma depletions form when they approach dawn.

[37] The merging process is illustrated in Figure 7. The plasma bubbles grow during the interval from T1 to T4. We assume that the maximum size (the width in the longitudinal direction) of each single bubble is ~100 km, consistent with the radar measurements and numerical simulations. In

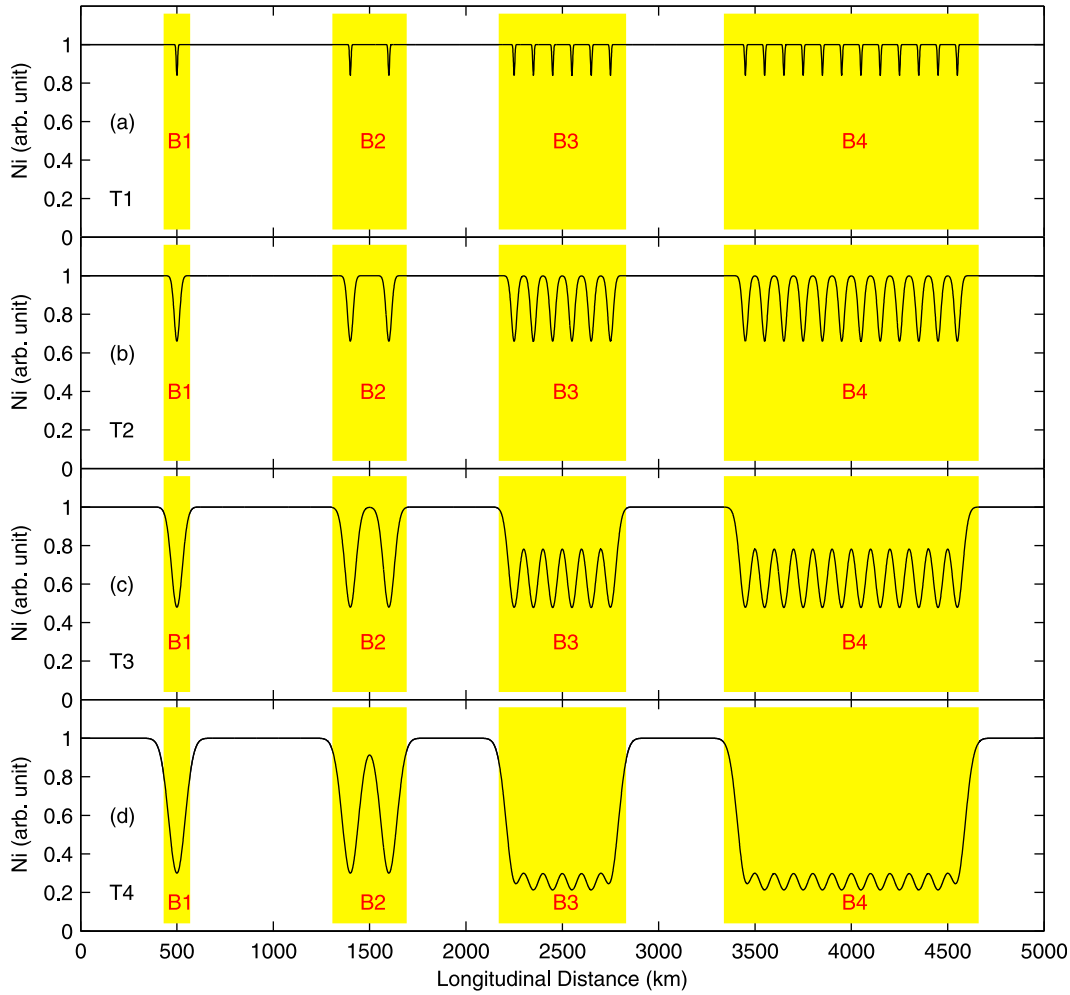

Figure 7. Illustration of the formation of wide plasma bubbles and broad plasma depletions through merging process. The plasma bubbles grow and become deeper and wider from time T1 to T4.

Figure 7, B1 represents an isolated plasma bubble. The bubble is very narrow at time T1 and grows to the maximum size at time T4. Because no other bubbles exist, only this single bubble will be detected in this region. B2 represents a family of two bubbles. These two bubbles are separated by 200 km in longitude. Each of the two bubbles grows to the maximum size of ~100 km at time T4. Because the maximum size is smaller than the longitudinal distance of the bubbles, the two bubbles are always separated. B3 represents a family of six bubbles. The longitudinal separation of successive bubbles is 100 km. The six bubbles are still separated at time T2, start to merge at time T3, and become a wide bubble at time T4. Note that the maximum width of each single bubble in B3 is the same (~100 km) as that in B1 and B2. However, when the width of the bubbles becomes comparable to the longitudinal separation of the bubbles, the merging process occurs and results in the formation of the wide bubble. The width of the wide bubble in B3 is ~600 km. B4 represents a family of twelve plasma bubbles, and the separation of successive bubbles is 100 km. Very similar to the process of B3, the twelve bubbles in B4 grow and merge to form a broad plasma depletion at time T4. The longitudinal coverage of the broad depletion in B4 is ~1200 km. The processes illustrated in Figure 7 can explain the occurrence of an isolated bubble, multiple separated bubbles, wide plasma bubbles, and broad plasma depletions.

[38] This scenario is consistent with the observations. In Figures 2c and 2d, the ion density and vertical velocity within the wide bubble, denoted by the yellow shading, are not smooth but show structures, suggesting the possible existence of multiple smaller bubbles. In Figures 5d and 5e, the ion vertical velocity inside the wide bubble appears to have three peaks, also suggesting the possible existence of three or more regular bubbles. The broad plasma depletions, denoted by the gray shading in Figures 2a and 2b, also consist of smaller-scale structures. The ion vertical velocity inside the depletion shows three large peaks, and the ion density shows corresponding enhancements. The longitudinal coverage of the entire broad depletion is ~20°. Each of the three ion velocity enhancements covers 6–7°, similar to the longitudinal width of the wide plasma bubbles. Furthermore, fine structures exist in the ion velocity in each velocity enhancement region, suggesting that each velocity enhancement over 6–7° may result from the merging of multiple plasma bubbles with smaller size.

[39] In this mechanism, the merging process of multiple bubbles is the key factor for the formation of wide plasma bubbles and broad plasma depletions. Multiple regular

bubbles (width of ~100 km) merge to form a wide bubble (width of up to 700 km as observed), and multiple wide bubbles further merge into a broad depletion (thousands of kilometers in longitude). The longitudinal width of the regular bubbles or wide bubbles must be continuously growing (becoming larger), so the merging of the regular bubbles into a wide bubble or into a broad depletion can occur. The ionospheric plasma is nearly incompressible. This mechanism does not require compressing the plasma between successive bubbles. When the width of individual bubbles becomes larger during the growth process, the plasma particles inside each bubble are moved upward and then flow to higher latitudes along the magnetic field lines. The widening of the bubbles is not an expansion process in longitude and does not compress the plasma.

[40] The observed growth time and decay time of the plasma bubbles are unusually long. The continuous growth of the plasma bubbles in the evening sector and the slow decay after midnight determines that most plasma bubbles become fully developed and are easily detected in the postmidnight sector. The plasma bubbles are caused by the Rayleigh-Taylor instability. The upward ion drift velocity inside each bubble is driven by polarization electric field and remains large after the bubbles have merged to form the wide bubble/broad depletion. An important property of the mechanism is the relation between equatorial plasma bubbles and broad plasma depletions: The broad plasma depletions result from merging of multiple plasma bubbles.

[41] This mechanism is different from those proposed earlier. *Huang et al.* [2009] used the cooling or downwelling process of the ionosphere and thermosphere to explain the generation of the broad plasma decreases near dawn and ruled out the possibility of plasma bubbles as the cause. In the simulations of *Huba et al.* [2010], the dawn plasma depletions are caused by an eastward electric field and also not related to plasma bubbles. The ion vertical velocity is small or weakly downward in the downwelling process of the ionosphere and is smaller than 30 m/s in the case of the eastward electric field effect. In our observations, the upward ion velocity reaches 300 m s^{-1} within the broad plasma depletion denoted by the gray shading in Figure 2b. The large upward ion velocity of 200–300 m s^{-1} in our case is the first major difference from the mechanisms proposed by *Huang et al.* [2009] and *Huba et al.* [2010]. The second major difference is the existence of plasma bubbles in our case. The upward ion velocity of 200–300 m s^{-1} is the typical signature of plasma bubbles caused by the Rayleigh-Taylor instability. We want to emphasize that we do not mean the mechanisms proposed by *Huang et al.* [2009] and *Huba et al.* [2010] are incorrect. Their interpretation is reasonable and valid for their cases. What we suggest is that the merging of multiple regular plasma bubbles can cause the formation of broad plasma depletions. The new mechanism can well explain why large upward ion drifts occur inside the depletion region.

[42] The formation of broad plasma depletions by the merging mechanism requires the existence of multiple plasma bubbles over a large longitudinal range. In the case reported by *Kelley et al.* [2009], a cluster of plasma bubbles were detected by C/NOFS over 30–40° in longitude. The new mechanism is consistent with the observations of *Kelley et al.* [2009]. However, we cannot determine how a series of plasma bubbles is generated over such a large distance. Atmospheric gravity waves [*Rottger*, 1973; *Kelley et al.*, 1981; *Huang et al.*, 1993; *Huang and Kelley*, 1996a, 1996b; *Abdu et al.*, 2009; *Takahashi et al.*, 2009; *Makela et al.*, 2010] and plasma shear flow [*Hysell et al.*, 2005a, 2005b, 2006; *Kudeki et al.*, 2007] in the bottomside *F* region are widely believed to be possible seed perturbations for ESF and plasma bubbles. In the cases presented in this paper, seed perturbations cannot be identified because of the altitude of C/NOFS. The Rayleigh-Taylor instability is excited in the bottomside *F* region. If the *F* peak altitude in the nighttime equatorial ionosphere is lower than the perigee (405 km) of C/NOFS, C/NOFS cannot directly detect perturbations in the bottomside *F* region. We have also not understood what determines the maximum size of plasma bubbles and under what ionospheric and thermospheric conditions the merging process is effective. It is not certain whether the formation of broad plasma depletions through merging of multiple plasma bubbles represent a peculiar phenomenon during deep solar minimum. Further investigations are required to solve these problems.

[43] In the case of 13 June 2008 (Figure 6), the plasma bubble becomes fully developed within ~100 min. This plasma bubble originates in the postmidnight sector and grows faster than those originating in the evening sector. The faster growth of the postmidnight bubble may be related to the density profile of the thermosphere. The atmosphere may move to low altitudes in the postmidnight sector during deep solar minimum. The ion-neutral collision frequency in the *F* region is low, and the growth rate of the Rayleigh-Taylor instability is high. As a result, plasma bubbles grow faster there. However, it should be mentioned that we propose this mechanism to explain the fast generation of the postmidnight plasma bubbles but do not have direct observations to verify that the atmosphere indeed moves to lower altitudes. This issue also requires further investigations.

4. Conclusions

[44] C/NOFS is a low-inclination satellite and can detect the same equatorial plasma bubble over successive orbits if the plasma bubble exists longer than the period of one complete orbit. The successive measurements of a plasma bubble can be used to trace the development of the bubble. We have analyzed the generation and evolution of plasma bubbles and broad plasma depletions observed by C/NOFS in three cases. The major conclusions are as follows.

[45] The plasma bubbles in two cases start to form in the evening sector. Ion density perturbations and enhanced upward ion velocity are first identified at ~2200 LT. The ion density perturbations are relatively weak before midnight and grow into fully developed plasma bubbles in the postmidnight sector. The observations show that the plasma bubbles observed in the midnight–dawn sector may originate in the evening sector.

[46] The C/NOFS measurements show that the size of the plasma bubbles is growing over two orbital periods (3.3 h). The Rayleigh-Taylor instability must have been excited in the bottomside *F* region at earlier time than it reaches the C/NOFS altitude, so the continuous growth time of the plasma bubbles is longer than 3.3 h. The ion vertical velocity inside the bubbles remains strongly upward for an additional

two orbits, and the bubbles do not decay significantly. The observations suggest that the decay time of the bubbles is also longer than 3.3 h.

[47] The plasma flow inside the bubbles is upward during the entire nighttime from evening to dawn. The bubbles do not become dead/fossil bubbles even when the bubbles reach ~0500 LT. The disappearance of the plasma bubbles is caused by the filling of newly produced plasma particles through photoionization process near dawn. The continuous growth of the plasma bubbles in the evening sector and the slow decay after midnight determines that most plasma bubbles become fully developed and are easily detected in the midnight–dawn sector.

[48] We propose a new mechanism to explain the generation of wide plasma bubbles and broad plasma depletions. A series of plasma bubbles starts to occur in the evening sector, and each of the bubbles is caused by the Rayleigh-Taylor instability. The longitudinal width of the plasma bubbles continuously grows during the rising process, so multiple bubbles with regular size can merge to form a wide bubble or a broad depletion. The upward ion drift velocity inside each individual regular bubble is driven by polarization electric field and remains large within the wide bubble/broad depletion region.

[49] **Acknowledgments.** Work by C.S.H. was supported by the Air Force Office of Scientific Research award FA9550-09-1-0321. The C/NOFS mission is supported by the Air Force Research Laboratory, the Department of Defense Space Test Program, the National Aeronautics and Space Administration, the Naval Research Laboratory, and the Aerospace Corporation.

[50] Robert Lysak thanks M. Keskinen and the other reviewers for their assistance in evaluating this paper.

References

Abdu, M., I. Batista, J. Sobral, E. de Paula, and I. Kantor (1985), Equatorial ionospheric plasma bubble irregularity occurrence and zonal velocities under quiet and disturbed conditions, from polarimeter observations, *J. Geophys. Res.*, *90*, 9921, doi:10.1029/JA090iA10p09921.

Abdu, M. A., I. S. Batista, H. Takahashi, J. MacDougall, J. H. Sobral, A. F. Medeiros, and N. B. Trivedi (2003), Magnetospheric disturbance induced equatorial plasma bubble development and dynamics: A case study in Brazilian sector, *J. Geophys. Res.*, *108*(A12), 1449, doi:10.1029/2002JA009721.

Abdu, M. A., E. Alam Kherani, I. S. Batista, E. R. de Paula, D. C. Fritts, and J. H. A. Sobral (2009), Gravity wave initiation of equatorial spread *F*/plasma bubble irregularities based on observational data from the SpreadFEx campaign, *Ann. Geophys.*, *27*, 2607, doi:10.5194/angeo-27-2607-2009.

Aggson, T. L., W. J. Burke, N. C. Maynard, W. B. Hanson, P. C. Anderson, J. A. Slavin, W. R. Hoegy, and J. L. Saba (1992), Equatorial bubbles updrafting at supersonic speeds, *J. Geophys. Res.*, *97*, 8581, doi:10.1029/92JA00644.

Burke, W. J., D. E. Donatelli, R. C. Sagalyn, and M. C. Kelley (1979), Low density regions observed at high altitudes and their connection with equatorial spread *F*, *Planet. Space Sci.*, *27*, 593, doi:10.1016/0032-0633(79)90157-0.

Burke, W. J., C. Y. Huang, C. E. Valladares, J. S. Machuzak, L. C. Gentile, and P. J. Sultan (2003), Multipoint observations of equatorial plasma bubbles, *J. Geophys. Res.*, *108*(A5), 1221, doi:10.1029/2002JA009382.

Burke, W. J., O. de La Beaujardiere, L. C. Gentile, D. E. Hunton, R. F. Pfaff, P. A. Roddy, Y.-J. Su, and G. R. Wilson (2009), C/NOFS observations of plasma density and electric field irregularities at postmidnight local times, *Geophys. Res. Lett.*, *36*, L00C09, doi:10.1029/2009GL038879.

de La Beaujardiere, O., et al. (2004), C/NOFS: A mission to forecast scintillations, *J. Atmos. Sol. Terr. Phys.*, *66*, 1573–1591, doi:10.1016/j.jastp.2004.07.030.

de La Beaujardiere, O., et al. (2009), C/NOFS observations of deep plasma depletions at dawn, *Geophys. Res. Lett.*, *36*, L00C06, doi:10.1029/2009GL038884.

Fejer, B. G., E. R. de Paula, S. A. González, and R. F. Woodman (1991), Average vertical and zonal *F* region plasma drifts over Jicamarca, *J. Geophys. Res.*, *96*, 13,901, doi:10.1029/91JA01171.

Fejer, B. G., L. Scherliess, and E. R. de Paula (1999), Effects of the vertical plasma drift velocity on the generation and evolution of equatorial spread *F*, *J. Geophys. Res.*, *104*, 19,859, doi:10.1029/1999JA900271.

Fejer, B. G., J. W. Jensen, and S.-Y. Su (2008), Quiet time equatorial *F* region vertical plasma drift model derived from ROCSAT-1 observations, *J. Geophys. Res.*, *113*, A05304, doi:10.1029/2007JA012801.

Haerendel, G. (1973), Theory of equatorial spread *F*, technical report, Max Planck Inst. fur Extraterr. Phys. Munich, Germany.

Hanson, W., and D. Bamgboye (1984), The measured motions inside equatorial plasma bubbles, *J. Geophys. Res.*, *89*, 8997, doi:10.1029/JA089iA10p08997.

Huang, C.-S., and M. C. Kelley (1996a), Nonlinear evolution of equatorial spread *F*: 1. On the role of plasma instabilities and spatial resonance associated with gravity wave seeding, *J. Geophys. Res.*, *101*, 283, doi:10.1029/95JA02211.

Huang, C.-S., and M. C. Kelley (1996b), Nonlinear evolution of equatorial spread *F*: 2. Gravity wave seeding of Rayleigh-Taylor instability, *J. Geophys. Res.*, *101*, 293, doi:10.1029/95JA02210.

Huang, C.-S., M. Kelley, and D. Hysell (1993), Nonlinear Rayleigh-Taylor instabilities, atmospheric gravity waves, and equatorial spread *F*, *J. Geophys. Res.*, *98*, 15,631, doi:10.1029/93JA00762.

Huang, C.-S., J. C. Foster, and Y. Sahai (2007), Significant depletions of the ionospheric plasma density at middle latitudes: A possible signature of equatorial spread *F* bubbles near the plasmapause, *J. Geophys. Res.*, *112*, A05315, doi:10.1029/2007JA012307.

Huang, C.-S., O. de La Beaujardiere, R. F. Pfaff, J. M. Retterer, P. A. Roddy, D. E. Hunton, Y.-J. Su, S.-Y. Su, and F. J. Rich (2010), Zonal drift of plasma particles inside equatorial plasma bubbles and its relation to the zonal drift of the bubble structure, *J. Geophys. Res.*, *115*, A07316, doi:10.1029/2010JA015324.

Huang, C. Y., F. A. Marcos, P. A. Roddy, M. R. Hairston, W. R. Coley, C. Roth, S. Bruinsma, and D. E. Hunton (2009), Broad plasma decreases in the equatorial ionosphere, *Geophys. Res. Lett.*, *36*, L00C04, doi:10.1029/2009GL039423.

Huba, J. D., and G. Joyce (2007), Equatorial spread *F* modeling: Multiple bifurcated structures, secondary instabilities, large density "bite-outs," and supersonic flows, *Geophys. Res. Lett.*, *34*, L07105, doi:10.1029/2006GL028519.

Huba, J. D., J. Krall, and G. Joyce (2009a), Atomic and molecular ion dynamics during equatorial spread *F*, *Geophys. Res. Lett.*, *36*, L10106, doi:10.1029/2009GL037675.

Huba, J. D., S. L. Ossakow, G. Joyce, J. Krall, and S. L. England (2009b), Three-dimensional equatorial spread *F* modeling: Zonal neutral wind effects, *Geophys. Res. Lett.*, *36*, L19106, doi:10.1029/2009GL040284.

Huba, J. D., G. Joyce, J. Krall, C. L. Siefring, and P. A. Bernhardt (2010), Self-consistent modeling of equatorial dawn density depletions with SAMI3, *Geophys. Res. Lett.*, *37*, L03104, doi:10.1029/2009GL041492.

Hysell, D. L., M. F. Larsen, C. M. Swenson, A. Barjatya, T. F. Wheeler, M. F. Sarango, R. F. Woodman, and J. L. Chau (2005a), Onset conditions for equatorial spread *F* determined during EQUIS II, *Geophys. Res. Lett.*, *32*, L24104, doi:10.1029/2005GL024743.

Hysell, D. L., E. Kudeki, and J. L. Chau (2005b), Possible ionospheric preconditioning by shear flow leading to equatorial spread *F*, *Ann. Geophys.*, *23*, 2647, doi:10.5194/angeo-23-2647-2005.

Hysell, D. L., M. F. Larsen, C. M. Swenson, A. Barjatya, T. F. Wheeler, T. W. Bullett, M. F. Sarango, R. F. Woodman, J. L. Chau, and D. Sponseller (2006), Rocket and radar investigation of background electrodynamics and bottom-type scattering layers at the onset of equatorial spread *F*, *Ann. Geophys.*, *24*, 1387, doi:10.5194/angeo-24-1387-2006.

Immel, T. J., S. B. Mende, H. U. Frey, L. M. Peticolas, and E. Sagawa (2003), Determination of low latitude plasma drift speeds from FUV images, *Geophys. Res. Lett.*, *30*(18), 1945, doi:10.1029/2003GL017573.

Kelley, M. C., M. Larsen, C. LaHoz, and J. McClure (1981), Gravity wave initiation of equatorial spread *F*: A case study, *J. Geophys. Res.*, *86*, 9087, doi:10.1029/JA086iA11p09087.

Kelley, M. C., R. C. Livingston, C. L. Rino, and R. T. Tsunoda (1982), The vertical wave number spectrum of topside equatorial spread *F*: Estimates of backscatter levels and implications for a unified theory, *J. Geophys. Res.*, *87*, 5217, doi:10.1029/JA087iA07p05217.

Kelley, M. C., et al. (1986), The Condor equatorial spread *F* campaign: Overview and results of the large-scale measurements, *J. Geophys. Res.*, *91*, 5487, doi:10.1029/JA091iA05p05487.

Kelley, M. C., J. J. Makela, L. J. Paxton, F. Kamalabadi, J. M. Comberiate, and H. Kil (2003), The first coordinated ground- and space-based optical observations of equatorial plasma bubbles, *Geophys. Res. Lett.*, *30*(14), 1766, doi:10.1029/2003GL017301.

Kelley, M. C., F. S. Rodrigues, J. J. Makela, R. Tsunoda, P. A. Roddy, D. E. Hunton, J. M. Retterer, O. de La Beaujardiere, E. R. de Paula, and R. R. Ilma (2009), C/NOFS and radar observations during a convective ionospheric storm event over South America, *Geophys. Res. Lett.*, *36*, L00C07, doi:10.1029/2009GL039378.

Keskinen, M. J., and S. L. Vadas (2009), Three-dimensional nonlinear evolution of equatorial ionospheric bubbles with gravity wave seeding and tidal wind effects, *Geophys. Res. Lett.*, *36*, L12102, doi:10.1029/2009GL037892.

Keskinen, M. J., S. L. Ossakow, and B. G. Fejer (2003), Three-dimensional nonlinear evolution of equatorial ionospheric spread *F* bubbles, *Geophys. Res. Lett.*, *30*(16), 1855, doi:10.1029/2003GL017418.

Krall, J., J. D. Huba, S. L. Ossakow, and G. Joyce (2010a), Why do equatorial ionospheric bubbles stop rising?, *Geophys. Res. Lett.*, *37*, L09105, doi:10.1029/2010GL043128.

Krall, J., J. D. Huba, G. Joyce, and T. Yokoyama (2010b), Density enhancements associated with equatorial spread *F*, *Ann. Geophys.*, *28*, 327, doi:10.5194/angeo-28-327-2010.

Kudeki, E., and S. Bhattacharyya (1999), Postsunset vortex in equatorial *F* region plasma drifts and implications for bottomside spread *F*, *J. Geophys. Res.*, *104*, 28,163, doi:10.1029/1998JA900111.

Kudeki, E., A. Akgiray, M. Milla, J. Chau, and D. Hysell (2007), Equatorial spread *F* initiation: Post-sunsent vortex, thermospheric winds, gravity waves, *J. Atmos. Sol. Terr. Phys.*, *69*, 2416, doi:10.1016/j.jastp.2007.04.012.

LaBelle, J., and M. C. Kelley (1986), The generation of kilometer-scale irregularities in equatorial spread *F*, *J. Geophys. Res.*, *91*, 5504, doi:10.1029/JA091iA05p05504.

Le, G., C. S. Huang, R. F. Pfaff, S. Y. Su, H. C. Yeh, R. A. Heelis, F. J. Rich, and M. Hairston (2003), Plasma density enhancements associated with equatorial spread *F*: ROCSAT-1 and DMSP observations, *J. Geophys. Res.*, *108*(A8), 1318, doi:10.1029/2002JA009592.

Makela, J. J., and M. C. Kelley (2003), Field-aligned 777.4-nm composite airglow images of equatorial plasma depletions, *Geophys. Res. Lett.*, *30*(8), 1442, doi:10.1029/2003GL017106.

Makela, J. J., S. L. Vadas, R. Muryanto, T. Duly, and G. Crowley (2010), Periodic spacing between consecutive equatorial plasma bubbles, *Geophys. Res. Lett.*, *37*, L14103, doi:10.1029/2010GL043968.

Miller, E. S., J. J. Makela, K. M. Groves, M. C. Kelley, and R. T. Tsunoda (2010), Coordinated study of coherent radar backscatter and optical airglow depletions in the central Pacific, *J. Geophys. Res.*, *115*, A06307, doi:10.1029/2009JA014946.

Park, S. H., S. L. England, T. J. Immel, H. U. Frey, and S. B. Mende (2007), A method for determining the drift velocity of plasma depletions in the equatorial ionosphere using far-ultraviolet spacecraft observations, *J. Geophys. Res.*, *112*, A11314, doi:10.1029/2007JA012327.

Pfaff, R., et al. (2010), Observations of DC electric fields in the low-latitude ionosphere and their variations with local time, longitude, and plasma density during extreme solar minimum, *J. Geophys. Res.*, *115*, A12324, doi:10.1029/2010JA016023.

Retterer, J. M. (2010a), Forecasting low-latitude radio scintillation with 3-D ionospheric plume models: 1. Plume model, *J. Geophys. Res.*, *115*, A03306, doi:10.1029/2008JA013839.

Retterer, J. M. (2010b), Forecasting low-latitude radio scintillation with 3-D ionospheric plume models: 2. Scintillation calculation, *J. Geophys. Res.*, *115*, A03307, doi:10.1029/2008JA013840.

Rottger, J. (1973), Wave-like structures of large-scale equatorial spread-*F* irregularities, *J. Atmos. Terr. Phys.*, *35*, 1195, doi:10.1016/0021-9169(73)90016-0.

Sahai, Y., et al. (2005), Effects of the major geomagnetic storms of October 2003 on the equatorial and low-latitude *F* region in two longitudinal sectors, *J. Geophys. Res.*, *110*, A12S91, doi:10.1029/2004JA010999.

Scannapieco, A. J., and S. L. Ossakow (1976), Nonlinear spread *F*, *Geophys. Res. Lett.*, *3*, 451, doi:10.1029/GL003i008p00451.

Su, Y.-J., J. M. Retterer, O. de La Beaujardiere, W. J. Burke, P. A. Roddy, R. F. Pfaff, G. R. Wilson, and D. E. Hunton (2009), Assimilative modeling of equatorial plasma depletions observed by C/NOFS, *Geophys. Res. Lett.*, *36*, L00C02, doi:10.1029/2009GL038946.

Takahashi, H., et al. (2009), Simultaneous observation of ionospheric plasma bubbles and mesospheric gravity waves during the SpreadFEx Campaign, *Ann. Geophys.*, *27*, 1477, doi:10.5194/angeo-27-1477-2009.

Tsunoda, R. T. (1983), On the generation and growth of equatorial backscatter plumes: 2. Structuring of the west walls of upwellings, *J. Geophys. Res.*, *88*, 4869, doi:10.1029/JA088iA06p04869.

Tsunoda, R. T., and B. R. White (1981), On the generation and growth of equatorial backscatter plumes: 1. Wave structure in the bottomside *F* layer, *J. Geophys. Res.*, *86*, 3610, doi:10.1029/JA086iA05p03610.

Tsunoda, R. T., R. C. Livingston, J. P. McClure, and W. B. Hanson (1982), Equatorial plasma bubbles: Vertically elongated wedges from the bottomside *F* layer, *J. Geophys. Res.*, *87*, 9171, doi:10.1029/JA087iA11p09171.

Valladares, C. E., R. Sheehan, S. Basu, H. Kuenzler, and J. Espinoza (1996), The multi-instrumented studies of equatorial thermosphere aeronomy scintillation system: Climatology of zonal drifts, *J. Geophys. Res.*, *101*, 26,839, doi:10.1029/96JA00183.

Woodman, R. F., and C. LaHoz (1976), Radar observations of *F*-region equatorial irregularities, *J. Geophys. Res.*, *81*, 5447, doi:10.1029/JA081i031p05447.

Zalesak, S. T., S. L. Ossakow, and P. K. Chaturvedi (1982), Nonlinear equatorial spread-*F*: The effect of neutral winds and background Pedersen conductivity, *J. Geophys. Res.*, *87*, 151, doi:10.1029/JA087iA01p00151.

J. O. Ballenthin, O. de La Beaujardiere, D. E. Hunton, and P. A. Roddy, Space Vehicles Directorate, Air Force Research Laboratory, 29 Randolph Rd., Hanscom AFB, MA 01731, USA.

C.-S. Huang and C. E. Valladares, Institute for Scientific Research, Boston College, 402 St Clement's Hall, 140 Commonwealth Ave., Chestnut Hill, MA 02467, USA. (chaosong.huang.ctr@hanscom.af.mil)

R. F. Pfaff, NASA Goddard Space Flight Center, Mail Code 674, Greenbelt, MD 20771, USA.